

# SANDIA REPORT

SAND98-2487  
Unlimited Release  
Printed November 1998

~~MS 0619 Review & Approval Desk,  
15102, for DOE/OSTI~~

## Designed Molecular Recognition Materials for Chiral Sensors, Separations and Catalytic Materials

RECEIVED  
DEC 07 1998  
OSTI

Tina M. Nenoff, Steven G. Thoma, Paula Provencio, Songling Jia, Jun Zhang,  
Yan Qiu, and John A. Shelnett

Prepared by  
Sandia National Laboratories  
Albuquerque, New Mexico 87185 and Livermore, California 94550

Sandia is a multiprogram laboratory operated by Sandia Corporation,  
a Lockheed Martin Company, for the United States Department of  
Energy under Contract DE-AC04-94AL85000.

Approved for public release; further dissemination unlimited.



**Sandia National Laboratories**

Issued by Sandia National Laboratories, operated for the United States Department of Energy by Sandia Corporation.

**NOTICE:** This report was prepared as an account of work sponsored by an agency of the United States Government. Neither the United States Government nor any agency thereof, nor any of their employees, nor any of their contractors, subcontractors, or their employees, makes any warranty, express or implied, or assumes any legal liability or responsibility for the accuracy, completeness, or usefulness of any information, apparatus, product, or process disclosed, or represents that its use would not infringe privately owned rights. Reference herein to any specific commercial product, process, or service by trade name, trademark, manufacturer, or otherwise, does not necessarily constitute or imply its endorsement, recommendation, or favoring by the United States Government, any agency thereof, or any of their contractors or subcontractors. The views and opinions expressed herein do not necessarily state or reflect those of the United States Government, any agency thereof, or any of their contractors.

Printed in the United States of America. This report has been reproduced directly from the best available copy.

Available to DOE and DOE contractors from  
Office of Scientific and Technical Information  
P.O. Box 62  
Oak Ridge, TN 37831

Prices available from (615) 576-8401, FTS 626-8401

Available to the public from  
National Technical Information Service  
U.S. Department of Commerce  
5285 Port Royal Rd  
Springfield, VA 22161

NTIS price codes  
Printed copy: A03  
Microfiche copy: A01



## **DISCLAIMER**

**Portions of this document may be illegible in electronic image products. Images are produced from the best available original document.**

SAND 98-2487  
Unlimited Release  
Printed November 1998

**Designed Molecular Recognition Materials for Chiral Sensors, Separations and  
Catalytic Materials**

Tina M. Nenoff, Steven G. Thoma, Paula Provencio, Songling Jia,  
Jun Zhang, Yan Qiu and John A. Shelnut  
Catalysis and Chemical Technologies Department &  
New Materials and Validation Department

Sandia National Laboratories  
P.O. Box 5800  
Albuquerque, NM 87185-0710

**ABSTRACT**

The goal is the development of materials that are highly sensitive and selective for chiral chemicals and biochemicals (such as insecticides, herbicides, proteins, and nerve agents) to be used as sensors, catalysts and separations membranes. Molecular modeling methods are being used to tailor chiral molecular recognition sites with high affinity and selectivity for specified agents. The work focuses on both silicate and non-silicate materials modified with chirally-pure functional groups for the catalysis or separations of enantiomerically-pure molecules. Surfactant and quaternary amine templating is being used to synthesize porous frameworks, containing mesopores of 30 to 100 angstroms. Computer molecular modeling methods are being used in the design of these materials, especially in the chiral surface-modifying agents. Molecular modeling is also being used to predict the catalytic and separations selectivities of the modified mesoporous materials. The ability to design and synthesize tailored asymmetric molecular recognition sites for sensor coatings allows a broader range of chemicals to be sensed with the desired high sensitivity and selectivity. Initial experiments target the selective sensing of small molecule gases and non-toxic model neural compounds. Further efforts will address designing sensors that greatly extend the variety of resolvable chemical species and forming a predictive, model-based method for developing advanced sensors.

## Table of Contents

Section	Page
Abstract	1
Introduction	3
Part I: Zinc Phosphate phases templated with the chiral organic molecule <i>d</i> -glucosamine	3
Part II a: Optical Reporter Groups for Sensing Chiral Chemicals	13
Part II b: A Pyridine-Sensitive Venus Flytrap Porphyrin	22
Distribution List	29

## Introduction

Chirality, or “handedness”, is four different groups attached to a carbon atom of a molecule that has two *nonsuperimposable mirror image* forms (each named enantiomer). The two forms of the chiral molecule can possess very different biological activity. Chiral synthesis and separations of both intermediate and final compounds are currently extremely important areas of research, especially for the chemical, pharmaceutical, agrochemicals, and biomedical industries.<sup>1</sup> In the pharmaceuticals industry (where chiral drug production alone is a \$40 billion/year business) rising drug development costs and regulatory requirements have translated into both slower licensing of new drugs and rapid rise in prescription drug costs. This industry is looking for both catalysts (where much work is focused on combinatorial chemistry approaches) and separations materials to greatly aid in the production of enantiomerically pure final products. The development of tunable, highly sensitive and selective molecular recognition materials for important chemical drug species will require enantioselective capabilities.

### I. Zinc Phosphate phases templated with the chiral organic molecule *d*-glucosamine.

In an effort to produce enantioselective materials, we have undertaken a study to design chiral inorganic molecular sieves. We have employed the knowledge and successes of recent work<sup>2-10</sup> by templating an inorganic structure with organic molecules. Zeolitic-type structures with chiral tetrahedral framework topologies have previously been synthesized.<sup>11-13</sup> Furthermore, chiral organometallic templates have been used to synthesize zeolitic and layered frameworks.<sup>14-16</sup> Amine molecules have been effective in templating zinc phosphates due to the readily available H-bonding between the nitrogen of the amine and the “dangling” hydroxide of terminal phosphate groups found on the walls of a pore.<sup>17,18</sup> The inherent need for an enantioselective framework, and our past experiences with nonaluminosilicate molecular sieves<sup>19-21</sup>, led us to study the zinc phosphate system. We have explored the transfer of size, shape and chirality of our templating molecule to the crystalline zinc phosphate system. The resultant materials from the synthetic approaches we describe are envisioned to either become enantioselective chromatography materials or be developed into membrane separations barriers.

## Experimental

### Synthesis of chirally templated Zinc Phosphate Phases.

The phase space explored for this work is defined by the ratios of zinc, phosphorus and hydroxide/template. The reactions are performed at room temperature, with reaction times of 3, 6 and 24 hours. The starting materials are 4M H<sub>3</sub>PO<sub>4</sub>, 25% wt. tetramethyl ammonium hydroxide (TMAOH) in water, *d*-glucosamine hydrochloride (C<sub>12</sub>H<sub>22</sub>N<sub>2</sub>O<sub>5</sub>•HCl; DGA; see figure 1) and 2M Zn(NO<sub>3</sub>)<sub>2</sub>.

Typical synthesis parameters for the *hexagonal phase* were as follows: 1.179g of 4M H<sub>3</sub>PO<sub>4</sub>, 3.6435g TMAOH, and 1.08g DGA are mixed in a capped Teflon bottle. To the clear solution is added 1.94g 2M Zn(NO<sub>3</sub>)<sub>2</sub>. The thixotropic mixture was shaken until milky and allowed to stand at room temperature. The phase precipitated out of a gel-like solution in 24 hours. The product was then recovered by vacuum filtration, washed repeatedly with de-ionized water, and allowed to dry in air. Typical synthesis parameters for the *layered*

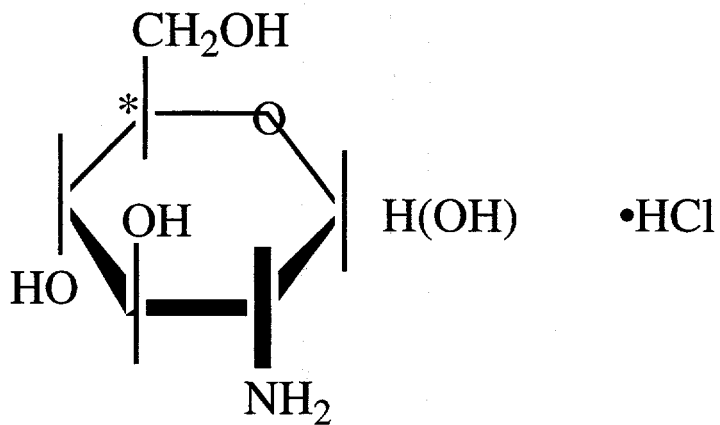
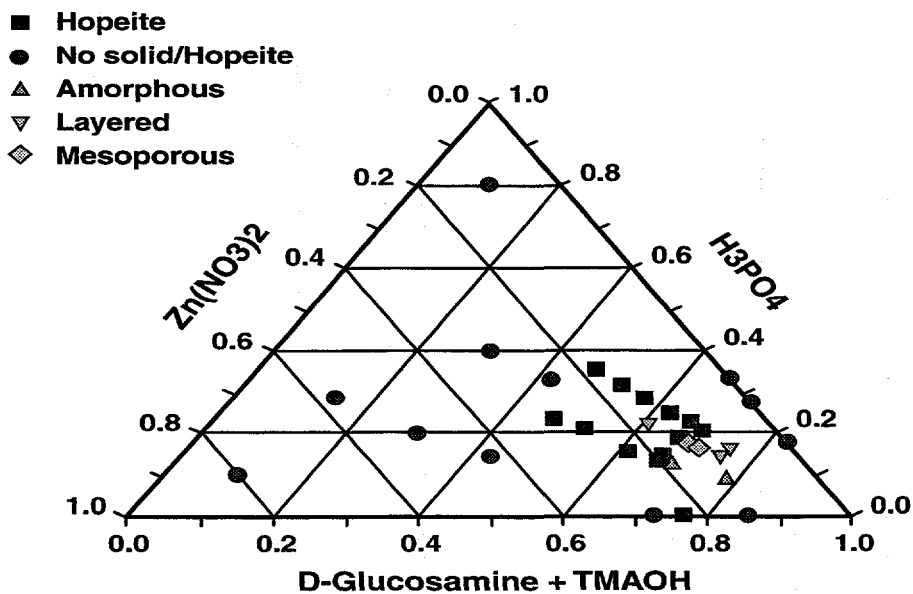


Figure 1 (above) : *d*-glucosamine hydrochloride.

Figure 2 (below) : Synthesis-space diagram of (*d*-glucosamine + TMAOH)/Zinc/Phosphate structures established by powder X-ray diffraction patterns.



*phase* were as follows: 1.179g of 4M H<sub>3</sub>PO<sub>4</sub>, 4.008g TMAOH, and 1.08g DGA are mixed in a capped Teflon bottle. To the clear solution is added 1.94g 2M Zn(NO<sub>3</sub>)<sub>2</sub>. The thixotropic mixture was shaken until milky and allowed to stand at room temperature. The phase precipitated out of a gel-like solution in 3 hours. For both crystalline phases, the template could not be removed by high vacuum at room temperature, calcination or solvent extraction (1M HCl/EtOH) without collapse of the structures. However, the template could be removed from the mesoporous phase after exposure to mild drying atmospheric conditions for long periods of time ( $\geq$  one month).

### Characterization

Powder X-ray diffraction data were collected at room-temperature on a Siemens Model D500 automated diffractometer, with  $\Theta$ - $2\Theta$  sample geometry and Cu K $\alpha$  radiation, between  $2\Theta = 5$  and  $60^\circ$ , step size  $0.05^\circ$ . Data presented were collected on "as synthesized" materials. **Transmission Electron Microscopy (TEM)** was performed on a JEOL 1200EX at 120 keV. Images were collected using a Gatan 694 retractable multiscan CCD camera. (Template was removed prior to TEM studies. Failure to remove template resulted in the structure "bursting", caused by electron beam heating of organic in pores.) **<sup>31</sup>P Cross-polarization magic angle spinning (CP/MAS)** and Bloch-decay MAS NMR data were acquired at 121.4Mhz on a Varian Unity Plus Spectrometer using a 7mm supersonic probe manufactured by Doty Scientific. Typical experimental parameters were 6.0kHz spinning speed, 6 $\mu$ s rf-pulse lengths ( $\pi/2$ -pulse for both <sup>31</sup>P and <sup>1</sup>H), and pre-pulse delays of 30s for CP/MAS experiments and between 120s and 600s for Bloch-decay experiments. <sup>1</sup>H decoupling was performed during all experiments.

### Results

Within the strict phase reaction limitations, we formed either (1) no precipitated phase; (2) Hopeite (Zn<sub>3</sub>(PO<sub>4</sub>)<sub>2</sub>•4H<sub>2</sub>O; a thermodynamically stable, small pored mineral); (3) a layered material (with intralayered distances of  $\approx 17\text{\AA}$ ); or (4) a mesoporous phase, with a hexagonal crystal lattice. (See figure 2) Note: layered materials of differing intralayer distances can be synthesized, depending on reaction conditions. Only one is presented here. (See figure 3.) Powder X-ray diffraction allowed us to identify and monitor the growth of different crystalline phases: a mesoporous phase (similar X-ray pattern to hexagonal MCM-41<sup>4</sup>), a layered phase and the Hopeite phase. (See figure 4) For "finger-printing" purposes, the identifiable peaks in the powder X-ray diffraction patterns ( $2\Theta = 1.5 - 10^\circ$ ) for the mesoporous, layered and Hopeite phases are  $d$  (in  $\text{\AA}$ ) = 31.223;  $d = 17.404$ ; and  $d = 9.141$ , respectively. The X-ray data is reinforced by TEM data. Distinct, measurable intralayer spacings on the interim layered phase, the mesoporous phase (see figure 5) and crystalline Hopeite are observed.

An investigation of the phase space indicates there is a very narrow range of reactants that provide for the synthesis of the mesoporous and layered phases. The phase space described here had a reaction time of 24 hours, with partial studies at 3 and 6 hour reaction times (to monitor phase growth). The reaction conditions studied indicate that 24 hours at room temperature will produce the mesoporous phase with reactants in the following ratio: 0.3H<sub>3</sub>PO<sub>4</sub> : 0.5Zn(NO<sub>3</sub>)<sub>2</sub> : 0.8(TMAOH + DGA). The layered phases were less well defined in ratio for crystallization, and tended to surround the region for mesoporous crystallization.

**10 nm**

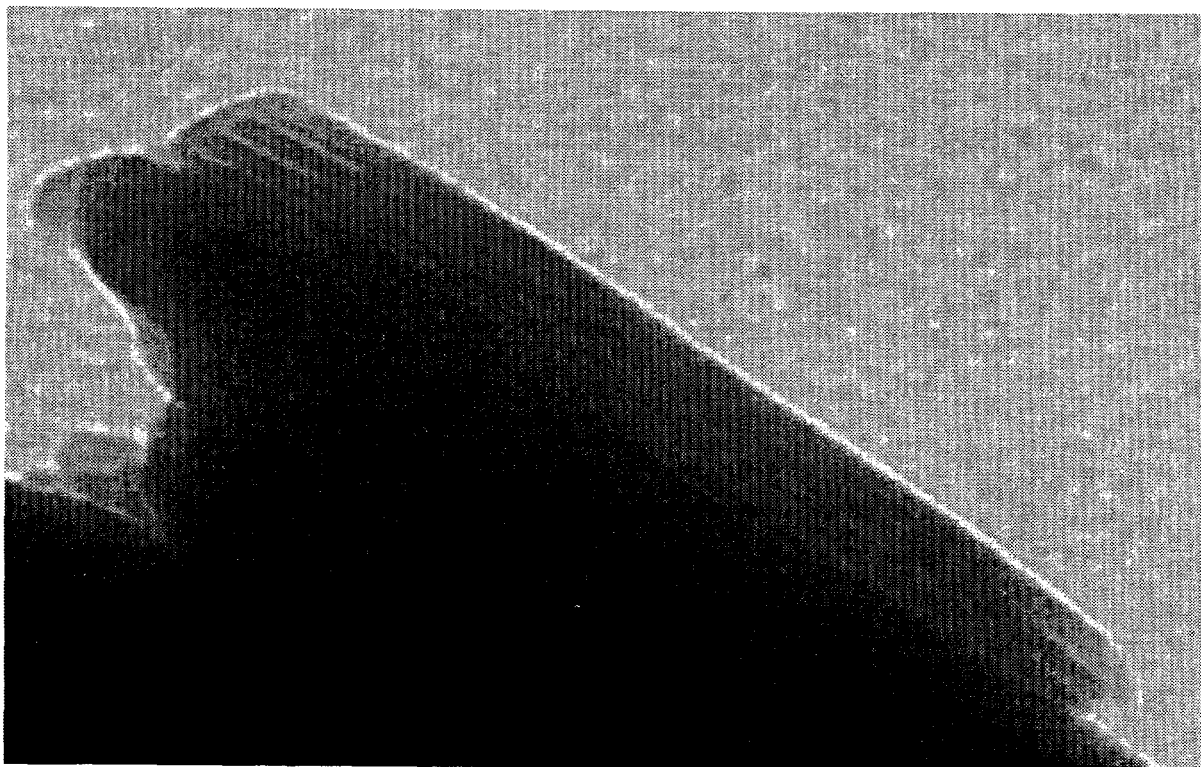


**Figure 3 (above) :** TEM of chirally templated zinc phosphate layered phase. Scale bar shown above.

**Figure 4 (below) :** Powder X-ray diffraction patterns of three phases synthesized in this phase space.

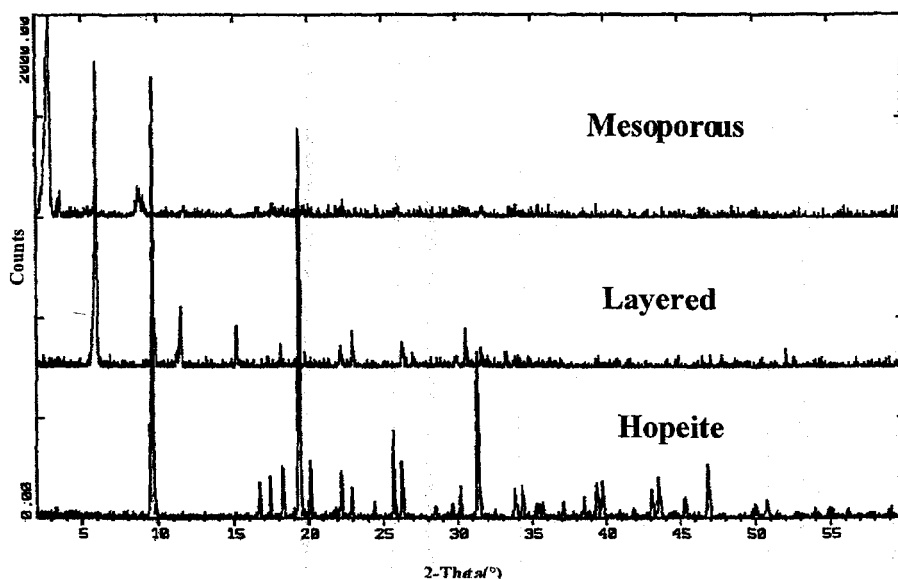
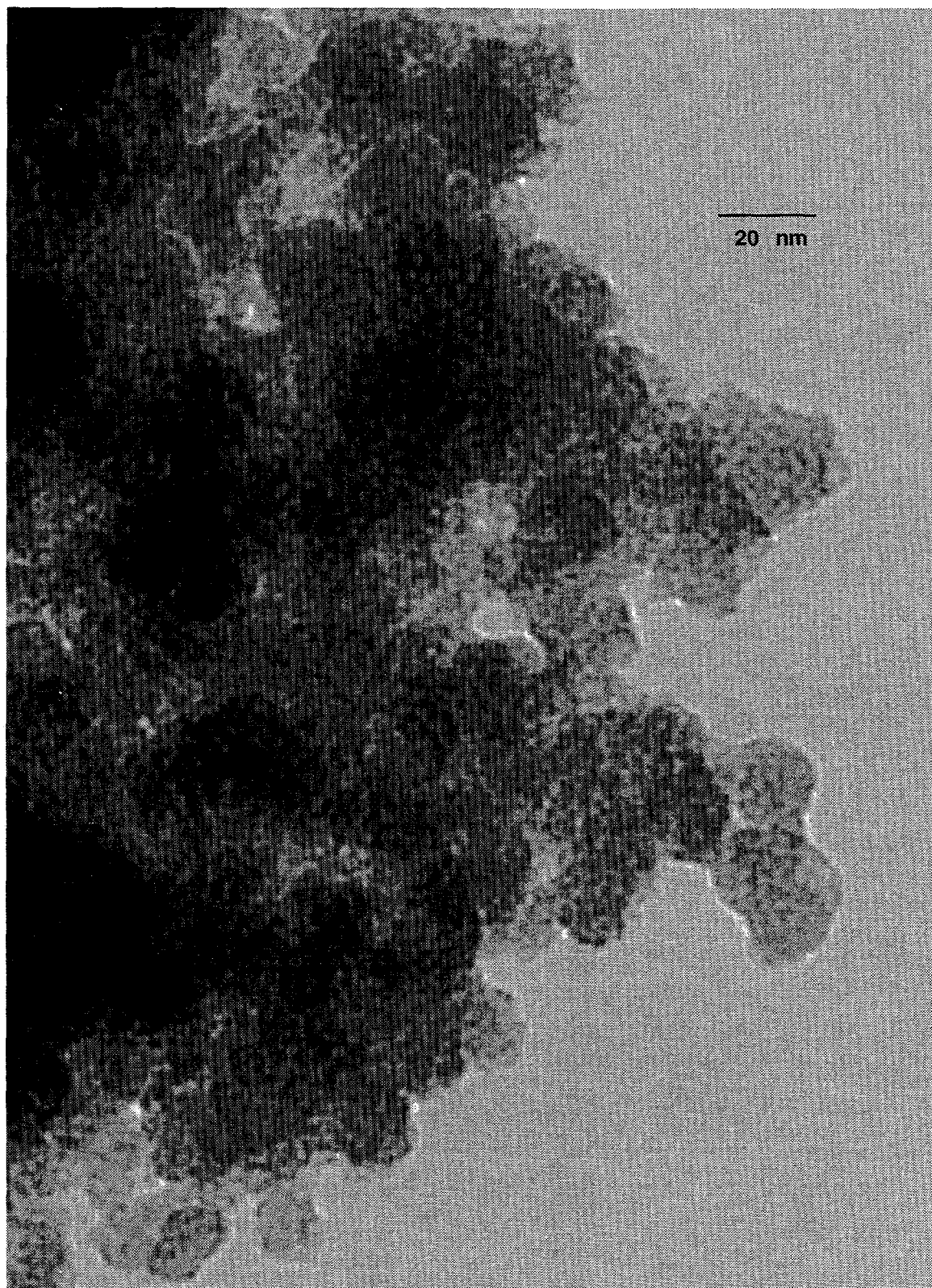


**Figure 5 :** TEM of chirally templated zinc phosphate mesoporous phase. The white spots are 32Å pores, the walls are zinc phosphate. The template was removed under mild vacuum with time. A scale bar is shown.



There are also distinct regions for Hopeite crystallization and no precipitation of a phase. We observed a transition in phase growth which is dependent on time of reaction. Much like was observed in the M41S studies<sup>6</sup> we observed an evolution of phase growth beginning with the interim layered templated-zinc phosphate phase (observed at 3 hours) with a primary  $d$  spacing of  $33 (\pm 1)$  Å. This layered phase disappears with an additional few hours of reaction time. After 24 hours of reaction, the mesoporous phase was observed, with identifiable  $d$  spacings of 35 and  $25 (\pm 1)$  Å. When the reaction was allowed to continue until 48 hours, Hopeite was the only crystallographic phase present. (See figure 6) The system appears to drive toward the thermodynamically stable, probably more favored, Hopeite phase.

Working in the zinc phosphate phase space, we found that we could synthesize a structure with a 3-dimensional pored system. Of particular interest to us was the TEM data. The coherent spacings were all approximately 32 Å, the pore sizes are consistent and the pores are distinct. Measurements of the repeat distance of the pores to be approximately 36 Å. This corresponds to  $2d_{100}/\sqrt{3}$  of the (100) peak (assignment of 31.2 Å powder X-ray diffraction peak to the (100); see figure 6). The remaining XRD peaks do not correspond to (110) or (200) peaks and may be due to impurity phases. There is a degree of shorter range ordering to the pores, however, there is a lesser degree of long range coherent crystalline pore ordering. Much like some water:co-solvent silica/surfactant disordered mesophases (d-H),<sup>22,23</sup> the liquid crystalline packing of the  $d$ -glucosamine molecules may have a disordered arrangement of cylindrical 1-d pores (quasi-hexagonal) that are intersecting disordered unimodal channels. Both systems exhibit similar long range disorder of the hexagonal packed pores in TEM images and the (100) diffraction peak in powder X-ray diffraction.

<sup>31</sup>P MAS NMR data indicate a crystalline framework for the mesoporous phase (as opposed to the all silicate MCM<sup>4,6</sup> mesoporous materials which have amorphous walls). The three peaks (8.0, 4.5 and 2.5 ppm chemical shifts) are all consistent with tetrahedral monophosphate species with varying degrees of distortion of the tetrahedral unit (see figure 7). The resonances are assigned as follows: the peaks at 8.0 and 4.5 ppm correspond to an impurity phase, consisting of Hopeite (4.5ppm) and an unknown Hopeite-related phase (8.0ppm), and the peak at 2.5 ppm attributed to the framework of the mesoporous phase. Note: the Hopeite-related phase is present only during and after NMR spinning (as monitored by XRD). The narrow peak widths (HWHM = 0.75 ppm) suggest, at most, a very small degree of variation in the geometry of the phosphate tetrahedra within the framework and thus show no evidence for the formation of an amorphous phosphate phase. Instead, data shows that the walls of this zinc phosphate mesoporous phase have an ordered arrangement of its tetrahedral atoms. Cross polarization and relaxation studies suggest that the mesoporous and Hopeite phases are phase separated on the nanometer scale or greater. The chemical shift for the mesoporous phase was found to be close to that of the <sup>31</sup>P MAS NMR data for crystalline ZnPO-X molecular sieves (5.8ppm).<sup>24</sup> The data strongly suggests the walls of this zinc phosphate mesoporous phase have an ordered arrangement of its tetrahedral atoms.

**Figure 6:** Powder X-ray diffraction patterns detailing the effect of time on reaction products. 3 hours = layered phase; 24 hours = mesoporous phase; 48 hours = Hopeite phase.

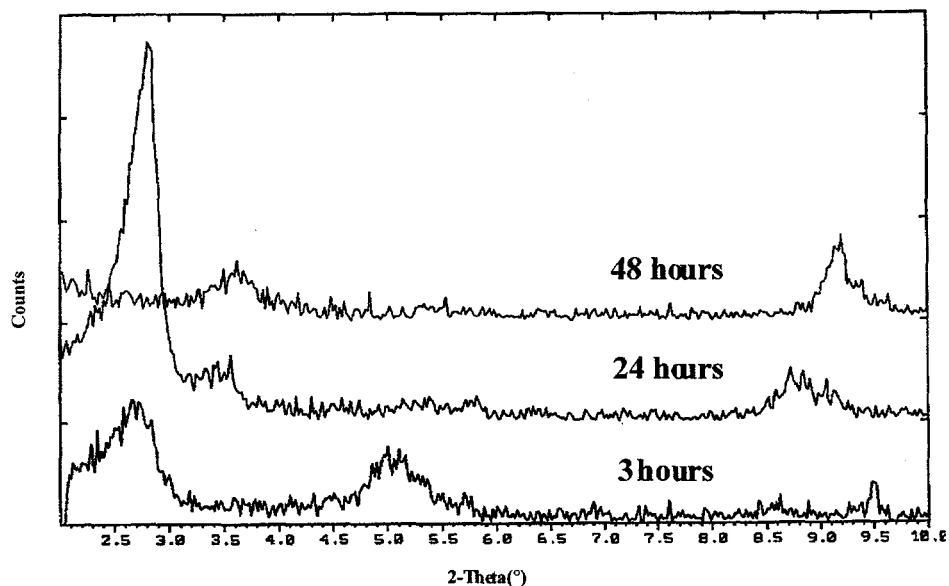
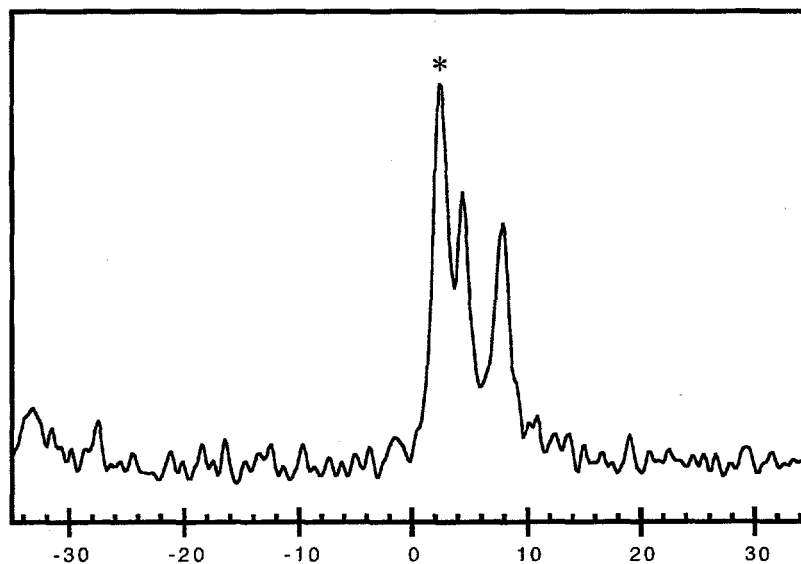


**Figure 7 :**  $^{31}\text{P}$  MAS NMR of mesoporous phase (with impurities), referenced to 85%  $\text{H}_3\text{PO}_4$ . (\*) indicates the mesoporous phase.



## Discussion

The ability to rapidly synthesize enantiomerically pure final products is clearly a desirable goal. However, this requires highly selective and active chiral catalysts. Typically, the asymmetric synthetic route to a drug or intermediate is so difficult that separation of the racemate turns out to be the cost-effective solution. The ability to design a chiral separations material is required. Furthermore, many drug molecules are larger than the average zeolitic pore ( $> 15\text{\AA}$ ) and therefore will be excluded from any separations. Chiral separations of large drug molecules through a chiral framework mesoporous phase should not be limited by the size of the drug molecules. With our mesoporous phase, the size of the pores and the possible chirality of the framework are important if this phase is to be used as a separations material.

Characterization results show that the zinc phosphate mesopore we describe is successfully templated by the chiral *d*-glucosamine hydrochloride. Powder X-ray diffraction data showed a hexagonally packed mesoporous phase, with short range coherent order. The  $^{31}\text{P}$  MAS NMR data indicated that the walls of the phase are crystalline and similar in local structure to Zn/P zeolite-analogs, as opposed to amorphous walls found in the silicate MCM mesopores phases. The single unidirectional pore size and shape of this mesopore also substantiates the possibility of chirality in the framework, in a fashion similar to the earlier predicted chiral polymorph of Zeolite B and of reported Co/P, -ABW, and -HEX phases.<sup>12,14</sup> With those reported materials, the crystallographic screw axis (which describes the chirality of the tetrahedral framework atoms) is shown to run in the direction of the channel system of the largest pore opening. Furthermore, by using one enantiomer of the chiral template in the reactions, we have attempted to ensure that structure direction will be enantiomerically pure.

The role of the chiral template is still being studied, so as to better understand how this small template is able to space fill extremely large intracrystalline voids. Much like the crystalline guanadine zinc phosphate phase reported by Harrison and Phillips<sup>18</sup>, it is possible that a number of DGA cations "cooperate" in a type of planar conformation, whereby they collectively are large enough to fill the  $31.2\text{\AA}$  pore of the mesoporous phase. In much the same way, hydrogen-bonding interactions between the amine group of the template to the oxygen atoms of the framework may account for the stability of the unit. However, there is also the possibility that protons from the hydroxyl groups of the sugar are weakly hydrogen bonding to the "dangling" phosphate groups of the framework. This would account for a much weaker interaction between the template and the framework. This theory is of interest to us because of our ability to remove the template through mild (long term) dehydration (see above), contrary to many amine templated zinc phosphate systems. Another theory for template geometry is that the *d*-glucosamine molecules are forming a large liquid crystalline (LC) cholesteric mesophase. This LC mesophase is comprised of helical aggregates of molecules, which contain a chiral center, and is referred to as a "twisted nematic mesophase".<sup>25</sup> In this case, chirality is maintained in the resulting superstructured template. Characterization and enantiomeric separation studies are on going to further resolve the issue of template molecular ordering.

## References

1. For more information see: *Chemical and Engineering News*, **71(39)**, 38 (1993); *Chemical and Engineering News* **72(38)**, 38 (1994); and Tombo, G. M. R.; Bellus, D. *Angew. Chem. Int. Ed. Engl.*, **30**, 1193 (1991).
2. Davis, M. E. *Acc. Chem. Res.* **1993**, *26*, 111.
3. Davis, M. E.; Lobo, R. L. *Chem. Mater.* **1992**, *4*, 756.
4. Kresge, C. T.; Leonowicz, M. E.; Roth, W. J.; Vartuli, J. C.; Beck, J. S. *Nature*, **1992**, *359*, 710.
5. Vartuli, J. C.; Kresge, C. T.; Leonowicz, M. E.; Chu, A. S.; McCullen, S. B.; Johnson, I. D.; Sheppard, E. W. *Chem. Mater.* **1994**, *6*, 2070.
6. Monnier, A.; Schuth, F.; Huo, Q.; Kumar, D.; Margolese, D.; Maxwell, R. S.; Stucky, G. D.; Krishnamurty, M.; Petroff, P.; Firouzi, A.; Janicke, M.; Chmelka, B. F. *Science*, **1993**, *261*, 1299.
7. Firouzi, A.; Kumar, D.; Bull, L. M.; Besier, T.; Sieger, P.; Huo, Q.; Walker, S. A.; Zasadzinski, J. A.; Glinka, C.; Nicol, J.; Margolese, D.; Stucky, G. D.; Chmelka, B. F. *Science*, **1995**, *267*, 1138.
8. Davis, M. E.; Zones, S. I., in *Synthesis of Microporous Materials: Zeolites, Clays and Nanostructures*, eds. M. L. Occelli and H. Kessler, Marcel Dekker, New York (1995).
9. Kubota, Y.; Helmkamp, M. M.; Zones, S. I.; Davis, M. E. *Microporous Materials*, **1996**, *6*, 213.
10. Stucky, G. D.; Huo, Q.; Firouzi, A.; Chmelka, B. F.; Schacht, S.; Voigt Martin, I. G.; Schuth, F. *Studies in Surface Science Cat.* **1997**, *105*, 3.
11. Harrison, W. T. A.; Gier, T. E.; Stucky, G. D.; Broach, R. W.; Bedard, R. A. *Chem. Mater.* **1996**, *8*, 145.
12. Newsam, J. M.; Treacy, M. M. J.; Koetsier, W. T.; de Gruyter, C. B. *Proc. R. Soc. London* **1988**, *A. 420*, 375.
13. Corma, A.; Iglesias, M.; del Pina, C.; Sanchez, F. *J. Chem. Soc., Chem. Commun.* **1991**, 1253.
14. Feng, P.; Bu, X.; Tolbert, S. H.; Stucky, G. D. *J. Am. Chem. Soc.* **1997**, *119*, 2497.
15. Bruce, D. A.; Wilkinson, A. P.; White, M. G.; Bertrand, J. A. *J. Solid State Chem.* **1996**, *125*, 228.
16. Ogunwumi, S. B.; Bein, T. *J. Chem. Soc., Chem. Commun.* **1997**, 901.
17. Harrison, W. T. A.; Nenoff, T. M.; Eddy, M. M.; Martin, T. E.; Stucky, G. D. *J. Mater. Chem.* **1992**, *2(11)*, 1127.
18. Harrison, W. T. A.; Phillips, M. L. F. *J. Chem. Soc., Chem. Commun.*, **1996**, 2771; Harrison, W. T. A.; Phillips, M. L. F. *Chem. Mater.* **1997**, *9*, 1837.
19. Nenoff, T. M.; Harrison, W. T. A.; Gier, T. E.; Stucky, G. D. *J. Amer. Chem. Soc.* **1991**, *113*, 378.
20. Gier, T. E.; Harrison, W. T. A.; Nenoff, T. M.; Stucky, G. D. in *Synthesis of Microporous Materials*, Vol. 1: Molecular Sieves, ed. M. L. Occelli and H. E. Robson, van Nostrand Reinhold, New York, **1992**, pp. 407-426.
21. Nenoff, T. M.; Miller, J. E.; Thoma, S. G.; Trudell, D. E. *Environ. Sci. Technol.* **1996**, *30*, 3630.
22. Anderson, M. T.; Martin, J. E.; Odinek, J. G.; Newcomer, P. P. *Chem. Mater.* **1998**, *10*, 311.

23. Ryoo, R.; Kim, J. M.; Ko, C. H.; Shin, C. H. *J. Phys. Chem.* **1996**, *100*, 17718.
24. Harrison, W. T. A.; Gier, T. E.; Moran, K. L.; Nicol, J. M.; Eckert, H.; Stucky, G. D. *Chem. Mater.* **1991**, *3*, 27.
25. Gibson, H. W. in *Liquid Crystals*, ed. F. D. Saeva, Marcel Dekker, Inc., New York, **1979**, pp. 99-162.

## II a. Optical Reporter Groups for Sensing Chiral Chemicals.

### Abstract

For chemical and biological sensing, molecular recognition centers that respond to the selective binding of chiral chemical species are needed. We are developing a novel type of chiral porphyrin as a chiral reporter group for chemical sensor devices. Molecular simulations are being used to guide the synthesis of these enantiomerically selective chiroporphyrin receptors for specified chiral substrates. One of the goals is to constrain the freedom of motion of functional groups attached at the periphery of the porphyrin ring to enable selective interactions of the chiroporphyrin with a target chiral species. An example of this type of chiroporphyrin receptor is zinc(II) heptabromo-mono-2-methoxyphenyl-tetraphenylporphyrin **1**; this porphyrin has no chiral atoms, but is chiral because of restricted rotation of the 2-methoxyphenyl substituent. The single methoxy group asymmetrically incorporated into the receptor promotes enantiomerically selective binding and hydrogen bonding to substrates, as shown by proton NMR spectroscopy.

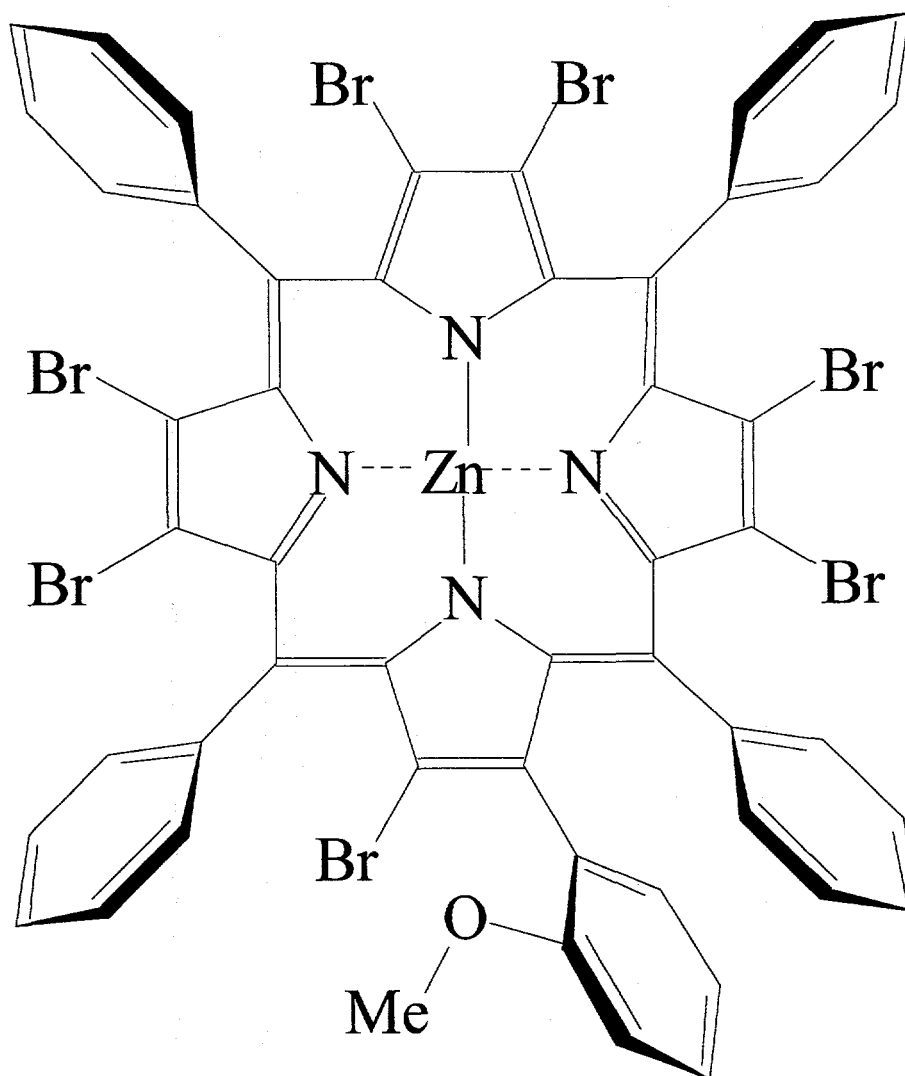
### Introduction

Many chemical and biological species that are of interest for chemical sensing are chiral. These materials include most biological materials, such as proteins and sugars, and many pharmaceuticals, herbicides, pesticides, and chemical and biological warfare agents. In principle, highly sensitive, selective, and specific recognition of these chemicals can be accomplished by computer design and synthesis of suitable molecular receptors.

The procedures for the synthesis of porphyrin derivatives have recently attained the richness and diversity required for the synthesis of highly elaborated superstructures that can be formulated as receptors for chiral chemical species. Currently, we are pursuing the goal of using molecular simulations to guide the synthesis of porphyrin-based receptors for chiral chemical species. Especially important in this regard is the advent of highly substituted nonplanar porphyrins<sup>1</sup>. The nonplanar porphyrins may resolve some of the recognized<sup>2</sup> difficulties associated with tailoring porphyrins for chiral recognition and catalysis. Besides their highly controllable structure, the most important property of porphyrins for sensor applications is their favorable optical properties (strong absorbance and emission, optical sensitivity to guest-host interaction). These optical properties can be used for self-reporting the substrate-binding event to the sensor device. For these reasons, we have used molecular mechanics to design a porphyrin receptor for chirally substituted pyrrolidines and piperidines.

Figure 1 shows a chiroporphyrin receptor designed by molecular simulation specifically for the selective binding of chiral amines, 2-pyrrolidinemethanol in particular. This initial choice for the target and receptor was influenced partly by the relative computational simplicity of the conformational search for the lowest-energy conformers. Specifically, the amine-chiroporphyrin complexes have severe steric constraints imposed by the crowding of the substituents at the porphyrin periphery, although even in this case about 100 stable conformers (local minima) can be calculated for the complexes. This comparative simplicity improves the likelihood of verifying the computational procedures and obtaining a clear preference for binding one enantiomer of the amine over the other. The desire for computational and chemical simplicity for our initial endeavor led us to design and synthesize

Figure 1: Zinc Chiroporphyrin 1.



the novel chiorporphyrin—zinc(II) heptabromo-mono-2-methoxyphenyl-*meso*-tetraphenylporphyrin. This porphyrin has no chiral atom but it is chiral because the rotational barrier for the methoxyphenyl group is large. In addition, the steric crowding of the peripheral substituents forces the porphyrin into a highly nonplanar conformation giving the chiral porphyrin enantiomers illustrated in Figure 2. It was hoped that this would also result in a highly constrained and enantioselective binding site at the metal center for various chiral amines. Indeed, this has been verified by proton NMR spectra, which have been interpreted with the aid of molecular simulations of the complexes formed between the porphyrin enantiomers and (S)-2-pyrrolidinemethanol.

### Experimental

Heptabromo-mono-2-methoxyphenyl-*meso*-tetraphenylporphyrin **1** was synthesized by a modified Suzuki coupling reaction<sup>3</sup>, using 2-methoxyphenyl-B(OH)<sub>2</sub> (5 equiv.), Pd[(PPh<sub>3</sub>)<sub>4</sub>] (0.15 equiv.), K<sub>2</sub>CO<sub>3</sub> (20 equiv.) in toluene at 90-100°C for two days. The racemic mixture was purified by column chromatography using silica gel and chloroform (60%)/hexane (40%). Zinc was inserted using Zn acetate in chloroform/methanol. The porphyrin enantiomers were then separated cleanly by chiral chromatography using a ChiralcelOD column eluted with 89:10:1 hexanes, chloroform, and isopropanol.

300-MHz proton-NMR spectra of the Zn porphyrins and pyrrolidine complexes were measured in toluene-d<sub>8</sub> at 193K. Molecular mechanics calculations were performed using a version of POLYGRAF (MSI) using a force field for metalloporphyrins developed over the last ten years and recently improved<sup>1,4</sup>.

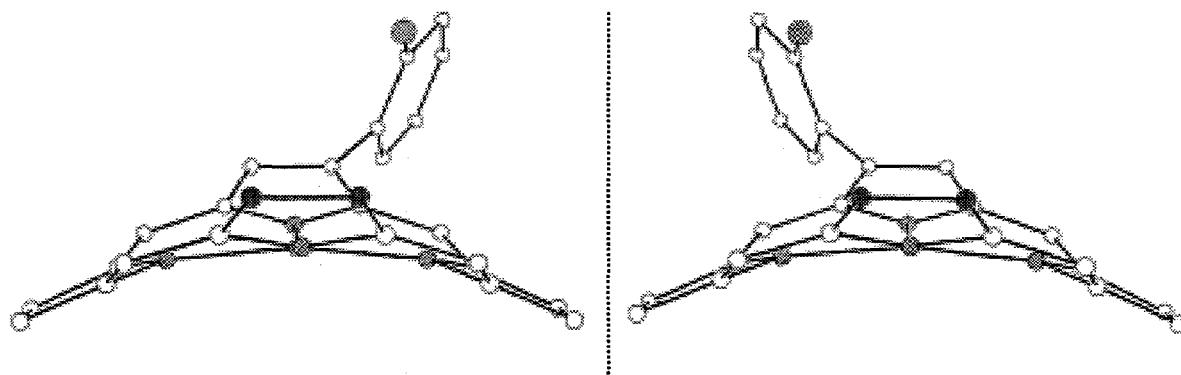
### 3. RESULTS AND DISCUSSION

The chiorporphyrin is obtained as a racemic mixture that can be separated by chiral chromatography. In solution, racemization of the individual enantiomers is very slow, taking days at room temperature. The molecular simulations indicate that simple analogs of chiorporphyrin **1** will completely inhibit racemization at room temperature. The Zn(II) chiorporphyrin derivative binds a single nitrogenous base to form a five-coordinate complex. Complexes with chiral derivatives of pyrrolidine and piperidine at the axial coordination sites of the metal give significant changes in the UV-visible absorption and emission spectra.

**Table 1.** *Energies (kcal/mol) of selected low-energy conformers of the (S)-2-pyrrolidinemethanol complexes with the chiorporphyrin enantiomers when the axial ligand and the methoxy group are on the same face of the porphyrin. Lowest energy conformers indicated in bold; H-bond energies in parenthesis.*

Complex	Rotational Isomer	Chiorporphyrin Enantiomer-1		Chiorporphyrin Enantiomer-2	
		<i>syn</i>	<i>anti</i>	<i>syn</i>	<i>anti</i>
<i>cis</i>	0°	<b>237.41</b> (-0.14)	244.00 (-2.85)	<b>237.18</b> (-3.52)	245.40 (-0.01)
	180°	<b>237.76</b> (-2.97)	245.21 (0.00)	<b>238.38</b> (-0.18)	244.61 (0.00)
<i>trans</i>	0°	238.64 (-0.18)	246.76(-0.06)	238.65 (-0.18)	249.74(-0.04)
	180°	238.54 (-0.18)	246.76(-0.06)	238.49 (-0.18)	249.88(-0.05)

**Figure 2 :** Zinc Chiroporphyrin enantiomers (mirror plane separates the two enantiomers).



Three major types of conformational isomers are calculated. First, the *cis* and *trans* complexes differ by whether the ligand and the methoxy groups are on the same (*cis*) or opposite (*trans*) face of the porphyrin ring. Second, the ligand can have different chiralities at the nitrogen atom; specifically, the NH hydrogen can be on the same side as the hydroxyl group (*syn*) or the opposite side (*anti*). Third, because of the saddle conformation of the porphyrin ring there are two preferred orientations of the ligand related by 180° rotation about the Zn-ligand bond. The 0° conformer is shown in Figure 3.

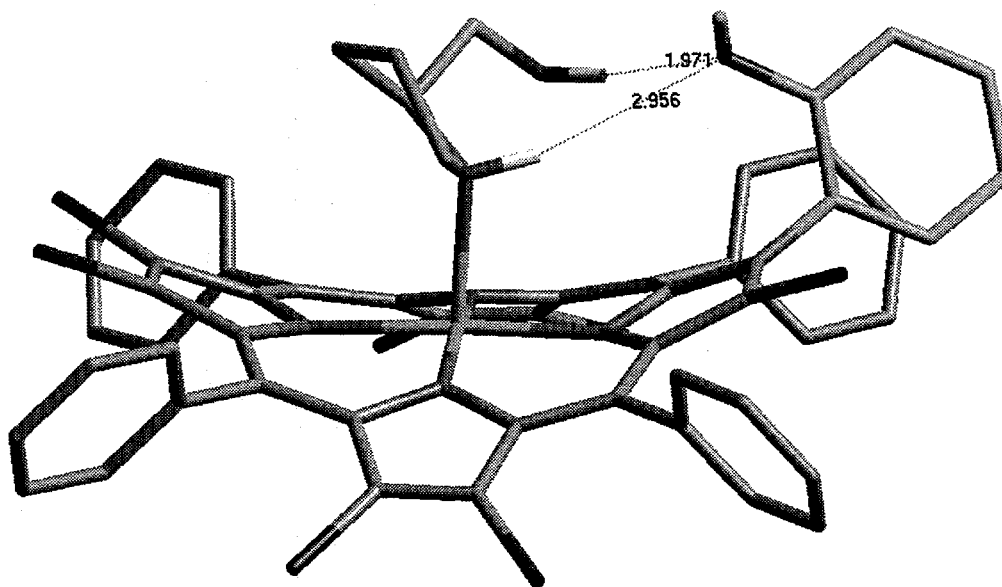
Table 1 lists the energies of selected conformers of the complexes between 2-pyrrolidinemethanol and the chiorporphyrin enantiomers for the *cis* complex. Compared with the *cis* complexes, the *trans* complexes are all at 238.5 kcal/mol or higher energy. Therefore, the calculations predict that, in the case of enantiomer-2, only the *cis*-0°-*syn* conformer (shown in Figure 3) is likely to be observed. In contrast for enantiomer-1, while the *cis*-*syn* configuration is still favored, both the 0°- and 180°-rotational isomers are energetically accessible. In addition, the *cis* configuration is less favored over the *trans* for enantiomer-1 so that both configurations may be observed.

The lowest energy *cis*-0°-*syn* complex of (S)-2-pyrrolidinemethanol with enantiomer-2 is shown in Figure 3. In this conformer, a strong hydrogen bond exists between the methoxy and hydroxyl groups, and a weaker H-bond exists between the N-H group and the methoxy group. The total H-bond energy is 3.5 kcal/mol, arising almost entirely from the hydroxyl H-bond. The H-bonds and coordination to the metal provide two of the three interactions necessary for enantiomeric selectivity. The groove formed by the saddle conformation of the ring gives a third steric interaction that provides enantiomeric selectivity. Note that the rotational barriers for the two lowest-energy rotational conformers were calculated to be 10.0 and 12.0 kcal/mol for the porphyrin enantiomers 1 and 2, respectively.

According to the calculations, enantiomer-2 is likely to form a specific complex in which only one rotational isomer of only the *cis* complex is observed. In contrast, at least two conformers should be present for enantiomer-1. This is in good agreement with the proton-NMR spectra of the chiorporphyrin complexes, shown in Figure 4 for the region encompassing the N-H proton of the (S)-2-pyrrolidinemethanol ligand. For comparison with the chiorporphyrin, the spectrum of Zn octabromo-*meso*-tetraphenyl-porphyrin (ZnBr<sub>8</sub>TPP) is shown at the bottom of Figure 4. This porphyrin is achiral, but simulates ligand binding to the *trans* face of the chiorporphyrin. The peak at -3.2 ppm is the NH proton of the axial ligand as shown by deuterium substitution; the two faces of the porphyrin are indistinguishable resulting in only one peak.

The spectrum of the complex of the porphyrin enantiomer that elutes at 12 minutes with (S)-2-pyrrolidinemethanol complex exhibits a NH doublet in the -3.2-ppm region and a second doublet near -3.0 ppm. We assign the doublet near -3.2 to the *trans* isomer in which the methoxy group and the ligand are on opposite faces of the porphyrin ring because of the similarity with the spectrum of ZnBr<sub>8</sub>TPP. The doublet at -3.0 ppm is assigned to the *cis* isomer, downshifted due to the ring current of the methoxyphenyl group and possibly weak H-bonding to the methoxy group. The doublets most likely result from 180°-rotational isomers of the ligand, as suggested by the molecular mechanics calculation, with the rotational isomers undergoing slow interconversion on the NMR time scale. For the 12-minute enantiomer, the NMR results indicate nonspecific binding of the ligand and only weak H-bonding of the ligand to the methoxy group. The NMR results for this porphyrin enantiomer are generally in agreement with the calculation for enantiomer-1, in that multiple *cis*

**Figure 3:** Lowest energy complex between 2-pyrrolidinemethanol and chiroporphyrin enantiomer-2.



conformers are observed. However, the calculations may slightly overestimate the energies of the *trans* forms since they are also observed.

The NMR spectrum of the complex with the enantiomer that elutes at 28 minutes exhibits only NH signals near -2.5 ppm. We attribute this to highly specific binding with significant H-bonding to the methoxy group as shown in Figure 3. This accounts for the large downfield shift of the NH proton. There is little evidence of ligand binding to the face opposite the methoxy group or for the 180° rotational isomer. The molecular simulations and the NMR results are consistent with enantiomer-2. The H-bonded *cis*-0°-*syn* form is highly favored over both the *trans* forms and the 180° isomer. In addition, NH hydrogen bonding is stronger than for enantiomer-1, accounting for the larger downfield shift.

The top spectrum in Figure 4 shows the spectrum of the chiorporphyrin racemate with (S)-2-pyrrolidinemethanol. One can rationalize this spectrum as a sum of the two individual porphyrin enantiomers.

## Conclusions

Proton-NMR results show that chiral amines can bind selectively to the chiorporphyrin enantiomers if a suitable fit is possible, otherwise nonspecific binding is observed. One enantiomer of 2-pyrrolidinemethanol binds in a highly specific fashion to one porphyrin enantiomer, while it binds to the other porphyrin enantiomer non-specifically. Equivalently, (S)-2-pyrrolidinemethanol binds specifically to enantiomer-2, while (R)-2-pyrrolidinemethanol binds nonspecifically to enantiomer-2. The chiorporphyrin receptor benefits from the nonplanarity of the porphyrin in two ways. First, the saddle structure acts to limit the rotational freedom of the axial ligand to two isomers related by a 180° rotation. Second, the nonplanarity brings the methoxy group closer to the axial ligand permitting the formation of the directing H-bond. Finally, the steric crowding of the substituents, which brings about the nonplanar structure, also limits the orientations of the methoxy chiral-resolving group to provide enhanced enantiospecificity. These results demonstrate the promise of designing highly specific receptors for chemical sensors using molecular simulations.

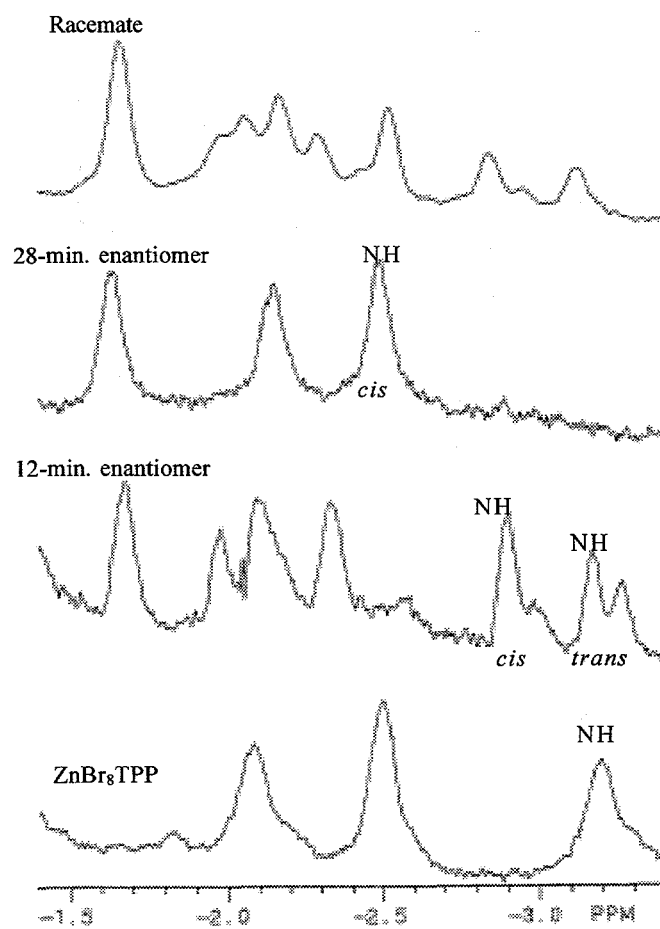
## References

1. J. A. Shelnut, X.-Z. Song, J.-G. Ma, S.-L. Jia, W. Jentzen, C. J. Medforth, *Chem. Soc. Rev.*, **1998**, 27, 31.
2. J. P. Collman, X. M. Zhang, V. J. Lee, E. S. Uffelman, J. I. Brauman, *Science*, **1993**, 261, 1404.
3. K. S. Chan, X. Zhou, B. Luo, *J. Chem. Soc., Chem. Commun.*, **1994**, 271.
4. X.-Z. Song, W. Jentzen, S.-L. Jia, L. Jaquinod, D. J. Nurco, C. J. Medforth, K. M. Smith, J. A. Shelnut, *J. Am. Chem. Soc.* **1996**, 118, 12975.

## Acknowledgments

This work was supported by the U.S. Department of Energy under Contract DE-AC04-94AL85000. Sandia is a multiprogram laboratory operated by Sandia Corporation, a Lockheed Martin Company, for the U. S. Department of Energy.

**Figure 4 :** NMR spectra of the chioroporphyrin enantiomers and  $ZnBr_8TPP$  with (S)-2-pyrrolidinemethanol in the NH region of the axial ligand.



## II b. A Pyridine-Sensitive Venus Flytrap Porphyrin

### Introduction

Metal complexes that drastically alter their shape upon binding of a ligand are not very common,<sup>1,2</sup> and very few have been fully characterized by X-ray structure determinations of both conformers. We report on an “open” zinc porphyrin host molecule that swings into a “closed” form upon binding a pyridine base. This conformational flip, which is reversible, is based on a rotation of the porphyrin substituents around their bonds to the *meso* positions; the X-ray structures of the two conformers show that it optimizes complementarity between host and guest (induced fit<sup>3</sup>). The description of this system as a pyridine-sensitive Venus flytrap<sup>1,4</sup> porphyrin readily comes to mind in view of its conceptual similarity to the insectivorous plant *Dionaea muscipula*.

The industrially available chiral cyclopropane derivative 1(*R*)-*cis*-hemicaldehyde<sup>5</sup> (“biocartol”) is a convenient source of low symmetry (*C*<sub>2</sub>) metal complexes of tetramethylchiorporphyrin (H<sub>2</sub>TMCP), which are useful prototypes of asymmetric catalysts and enantioselective receptors.<sup>1,6</sup> In the view of promoting attractive *π-π* interactions<sup>1,7</sup> between ester substituents and aromatic ligands, the *m*- and *p*-nitrophenyl esters of 1(*R*)-*cis*-caronaldehydic acid were synthesized<sup>8</sup> and condensed with pyrrole to afford the corresponding tetra-*m(p)*-nitrophenylchiorporphyrins H<sub>2</sub>T-*m*-NPCP (**1**) and H<sub>2</sub>T-*p*-NPCP (**2**) in 5-10% yield. In both cases, this atroposelective cyclization affords the  $\alpha\beta\alpha\beta$  atropisomer as the sole porphyrin product. The latter is then smoothly converted to its zinc complex, [Zn(EtOH)(T-*m*-NPCP)] (**3**) or [Zn(EtOH)(T-*p*-NPCP)] (**4**), respectively,<sup>9</sup> by reaction with zinc acetate in refluxing chloroform-ethanol (1:1). No atropisomerization occurs under these conditions, indicating that the bulky cyclopropyl groups prohibit rotation of the *meso* substituents.

The crystal structure of **3**<sup>10</sup> confirms the open conformation and the *C*<sub>2</sub> symmetry with the 2-fold axis running through the mean plane of the highly ruffled porphyrin (Figure 1). The zinc center and its ethanol axial ligand are therefore disordered over two equivalent positions. In addition, there are two different ethanol conformers for each position. The ethanol oxygen atom is at a long hydrogen-bonding distance to the carbonyl group. The conformation of the ester groups is such that the four carbonyl oxygen atoms are in positions nearly eclipsing the four R pyrrole carbon atoms C(a<sub>2</sub>), C(a<sub>3</sub>), C(a<sub>3</sub>)', and C(a<sub>2</sub>)', thereby pushing the *m*-nitrophenyl groups to the periphery of the porphyrin and nearly perpendicular to its mean plane. The similarity of <sup>1</sup>H NMR spectra for **3** and **4**, and particularly the absence of a notable porphyrin ring current effect on the phenyl resonances, suggests analogous conformations of the nitrophenyl ester groups of **3** and **4** in solution.

Addition of an equivalent of 3,5-lutidine to a CDCl<sub>3</sub> solution of **4** results in an immediate and complete switching from the open  $\alpha\beta\alpha\beta$  conformation to the closed, axially

ligated  $\alpha\alpha\alpha\alpha$  form. This flipping is conveniently monitored by the change of multiplicity of the pyrrolic proton NMR resonances from a  $D_2$ -symmetric to a  $C_4$ -symmetric pattern<sup>11</sup>.

Pyridine, 4-methylpyridine, and piperidine all induce a qualitatively similar effect, but the conversion to the closed form is incomplete and the  $\alpha\alpha\alpha\beta$  atropisomer is formed as well to varying degrees. Addition of hydrochloric acid to a solution of the closed  $\alpha\alpha\alpha\alpha$  conformer opens the flytrap, affording the  $\alpha\beta\alpha\beta$  atropisomer. Crystals of X-ray quality were obtained by diffusion of pyridine into a solution of **4** at room temperature. The pyridine adduct [Zn(py)(T-*p*-NPCP)] (**5**) exhibits the  $\alpha\alpha\alpha\alpha$  conformation (Figure 2). Its unusual stereochemical features give a clue to the origin of this conformational switching. The porphyrin macrocycle is highly  $C_4V$  domed, and the plane of the pyridine ligand is in eclipsed orientation with a N-Zn-N axis. The coordinated pyridine is tightly sandwiched between a pair of nearly parallel *p*-nitrophenyl groups by double *II-II* stacking (*d* center-center *ca.* 3.5 Å), while the other pair is nearly perpendicular and exhibits edge-to-face interactions with it (*d* center-center = 5.0 and 5.5 Å). A single carbonyl group, C(16)-O(1), shows the usual “inward” orientation, while the other three are directed radially outward.

The energy landscape revealed by molecular mechanics calculations is very complex, but some general conclusions can be drawn. The macrocycles of the  $\alpha\alpha\alpha\alpha$  conformers are predominantly domed and the  $\alpha\beta\alpha\beta$  conformers are predominantly ruffled, in agreement with the crystal structures. For the pyridine complex, the lowest-energy  $\alpha\alpha\alpha\alpha$  conformer for any specific arrangement of the carbonyls is always lower in energy (*ca.* 1 kcal/mol) than the corresponding  $\alpha\beta\alpha\beta$  conformer.

This energy gain provides a plausible driving force for the  $\alpha\beta\alpha\beta \rightarrow \alpha\alpha\alpha\alpha$  atropisomer conversion. In contrast, for the ethanol complex, the  $\alpha\beta\alpha\beta$  conformer is more stable (by *ca.* 2 kcal/mol) than the  $\alpha\alpha\alpha\alpha$  conformer. The preference of these ligands for either conformer is probably the combined effect of (a) a minimization of the steric repulsion between the substituents and the axial ligand and (b) a maximization of their attractive van der Waals interactions by favorable packing. The predicted preference of ethanol and pyridine for a particular conformer is carried over into the crystal environment. Structural decomposition of both the calculated and X-ray structures of the pyridine complex into contributions from ruffling, saddling, doming, and waving distortions<sup>12</sup> shows that the macrocycle is almost purely domed. This domed conformation also favors the eclipsed ligand orientation which is observed in the crystal structure.

The apparent lower rotation barrier of the porphyrin substituents in the presence of pyridine bases deserves further investigation. Our current interpretation, based on the crystal structures, is that the highly domed conformation of the porphyrin, which results from strong binding of pyridine (Zn-N: 2.119 Å), allows fast *meso* group rotation at room temperature and attainment of a dynamic equilibrium between atropisomers.

In contrast, weak ethanol ligation results in a long Zn-O bond (2.227 Å) and in a ruffled porphyrin conformation which inhibits *meso* group rotation. Molecular mechanics calculations provide significantly lower estimates for the  $\alpha\alpha\alpha\alpha \rightarrow \alpha\alpha\alpha\beta$  rotation barrier of the domed porphyrin complex (26-35 kcal/mol) than for the  $\alpha\beta\alpha\beta \rightarrow \alpha\alpha\alpha\beta$  transition of the ruffled conformer (30-45 kcal/mol).

It is noteworthy that the degree of flipping induced by pyridine and its derivatives parallels their substituent electron-releasing properties (3,5-lutidine > 4-methylpyridine > pyridine), in keeping with the electrostatic component of  $\Pi$ - $\Pi$  interaction and the known electron donor-acceptor arene complexation chemistry.<sup>1,13</sup> The flipping ability of the host substituents (*p*-nitrophenyl > *m*-nitrophenyl) follows the same trend. On the other hand, the lower effect of piperidine (pyridine > piperidine) is likely to reflect a less-than-ideal fit of this guest in a chair conformation relative to the flat aromatic core of pyridine. The observed ranking of guests suggests that the driving force for the  $\alpha\beta\alpha\beta \rightarrow \alpha\alpha\alpha\alpha$  conversion is enthalpic (the entropic change is similar) and arises from more favorable interactions between host and guest.

We note that the ligand-triggered  $\alpha\beta\alpha\beta \rightarrow \alpha\alpha\alpha\alpha$  conversion could in principle bring together and align appropriate reactive or catalytic groups, as well as provide a mechanism for the controlled delivery of pyridine-containing drugs. Its utility in the creation of shape-selective and chiral oxygenation catalysts, and of hemoprotein analogues, will also be explored.

## References:

- (1) A full list of references is supplied in our published literature.
- (2) Vernik, I.; Stynes, D. V. *Inorg. Chem.* **1996**, *35*, 6210.
- (3) Koshland, D. E. *Angew. Chem., Int. Ed. Engl.* **1994**, *33*, 2375.
- (4) Paxton, R. J.; Beatty, B. G.; Hawthorne, M. F.; Varadarajan, A.; Williams, L. E.; Curtis, F. L.; Knobler, C. B.; Beatty, J. D.; Shively, J. E. *Proc. Natl. Acad. Sci. U.S.A.* **1991**, *88*, 3387.
- (5) Martel, J. The Development and Manufacture of Pyrethroid Insecticides. In *Chirality in Industry*; Collins, A. N., Sheldrake, G. N., Crosby, J., Eds.; Wiley: Chichester, 1992; pp 87-109.

- (6) (a) Veyrat, M.; Maury, O.; Faverjon, F.; Over, D.; Ramasseul, R.; Marchon, J. C.; Turowska-Tyrk, I.; Scheidt, W. R. *Angew. Chem., Int. Ed. Engl.* **1994**, *33*, 220. (b) Mazzanti, M.; Veyrat, M.; Ramasseul, R.; Marchon, J. C.; Turowska-Tyrk, I.; Scheidt, W. R. *Inorg. Chem.* **1996**, *35*, 3733.
- (7) Hunter, C. *Chem. Soc. Rev.* **1994**, 101.
- (8) Veyrat, M.; Fantin, L.; Desmoulins, S.; Petitjean, A.; Mazzanti, M.; Ramasseul, R.; Marchon, J. C.; Bau, R. *Bull. Soc. Chim. Fr.* **1997**, *134*, 703.
- (9) Synthetic, spectroscopic, and crystallographic information is provided in our published literature.
- (10) Crystal data for [3] $\beta$ 1.02CH<sub>2</sub>Cl<sub>2</sub>: orthorhombic, space group *P21212*,  $a = 20.6871(11)$  Å,  $b = 13.8718(14)$  Å,  $c = 12.3315(9)$  Å,  $V = 3538.9(4)$  Å<sup>3</sup>, and  $Z = 2$ ; 26 031 reflections were collected and appropriately averaged, 9 9263 of which were unique ( $130$  K,  $2.21^\circ < \theta < 29.87^\circ$ ); 7953 reflections [ $I > 2\theta(I)$ ] yield  $R = 0.0661$  and  $R_w = 0.1866$ . *Note*: the ideal formula is [3]  $a = 2.0$  CH<sub>2</sub>Cl<sub>2</sub> and the total population of the solvent sites accidentally is very near one, as the two sites are effectively together only half-filled. Crystal data for [5]  $\beta = 2.71$ CH<sub>2</sub>Cl<sub>2</sub>: monoclinic, space group *P21*,  $a = 15.065(2)$  Å,  $b = 13.986(1)$  Å,  $c = 17.565(3)$  Å,  $\beta = 101.590(7)^\circ$ ,  $V = 3625.5(8)$  Å<sup>3</sup>, and  $Z = 2$ ; 27 411 reflections were collected and appropriately averaged, 9 12 530 of which were unique ( $127$  K,  $2.18^\circ < \theta < 29.85^\circ$ ); 10 963 reflections [ $I > 2\theta(I)$ ] yield  $R = 0.055 12$  and  $R_w = 0.1299$ . *Note*: the ideal formula is [5] $\beta$ 3.0CH<sub>2</sub>Cl<sub>2</sub> and the refined 2.72 population of the solvent sites reflects an attempt to properly account for partially occupied solvent sites.
- (11) Le Maux, P.; Bahri, H.; Simonneaux, G. *Tetrahedron* **1993**, *49*, 1401.
- (12) Jentzen, W.; Song, X.-Z.; Shelnut, J. A. *J. Phys. Chem. B* **1997**, *101*, 1684.
- (13) Ferguson, S. B.; Sanford, E. M.; Seward, E. M.; Diederich, F. *J. Am. Chem. Soc.* **1991**, *113*, 5410.

**Acknowledgment.** Work at CEA-Grenoble was supported by the CNRS (grant URA 1194), that at Notre Dame by the NIH (grants GM-38401 and RR-06709), and that at Sandia by the DOE (contract DE-AC04-94AL8500). M. Mazzanti thanks the European Union for a postdoctoral fellowship. We thank M. Veyrat, R. Ramasseul, and M. Bardet for helpful discussions, S. Desmoulins, C. Lebrun, and F. Sarrazin for assistance, and Roussel Uclaf for a gift of biocartol.

**Supporting Information Available:** Synthetic schemes for **1** and **2**, 400 MHz  $^1\text{H}$  NMR spectra of **4** and of **4** in the presence of 1 equiv of 3,5-lutidine, and X-ray structural information on **3** and **5** (54 pages). An X-ray crystallographic file, in CIF format, is available through the Internet only. See any current masthead page for ordering and Internet access instructions.

**Figure 1.** ORTEP view (50% probability) of the X-ray structure of the zinc chiroporphyrin [Zn(EtOH)(T-*m*-NPCP)] **3** showing the  $\alpha\beta\alpha\beta$  conformation of the host and ethanol guest.

**Figure 2.** ORTEP view (50% probability) of the X-ray structure of the zinc chiroporphyrin [Zn(py)(T-*p*-NPCP)] **5** showing the  $\alpha\alpha\alpha\alpha$  conformation of the host in the presence of the pyridine guest. The coordinated pyridine is tightly sandwiched between a pair of nearly parallel *p*-nitrophenyl groups by double face-to-face  $\pi$ - $\pi$  stacking, while the other pair is nearly perpendicular and exhibits edge-to-face interactions with it.

**Figure 1**

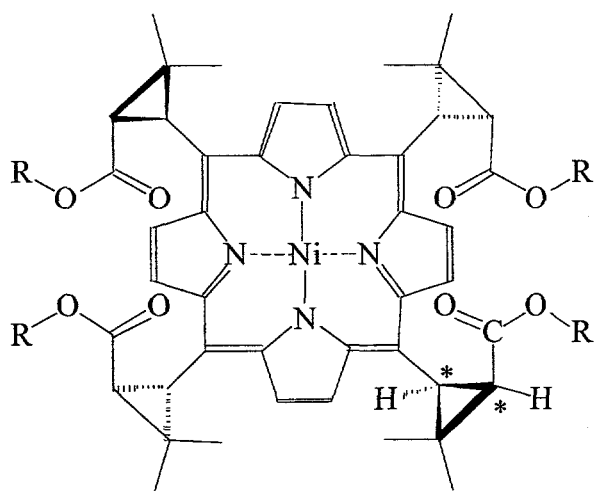
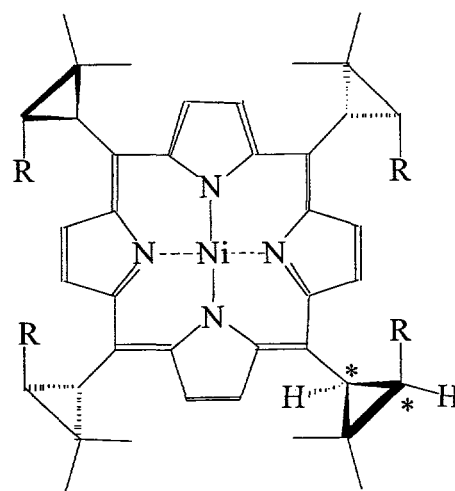


**Figure 2**



Substituent groups on above porphyrins can be R =

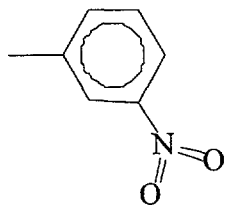
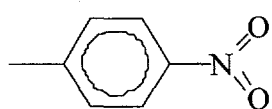


**Figure 3:** Open configuration of “Venus Flytrap” porphyrin

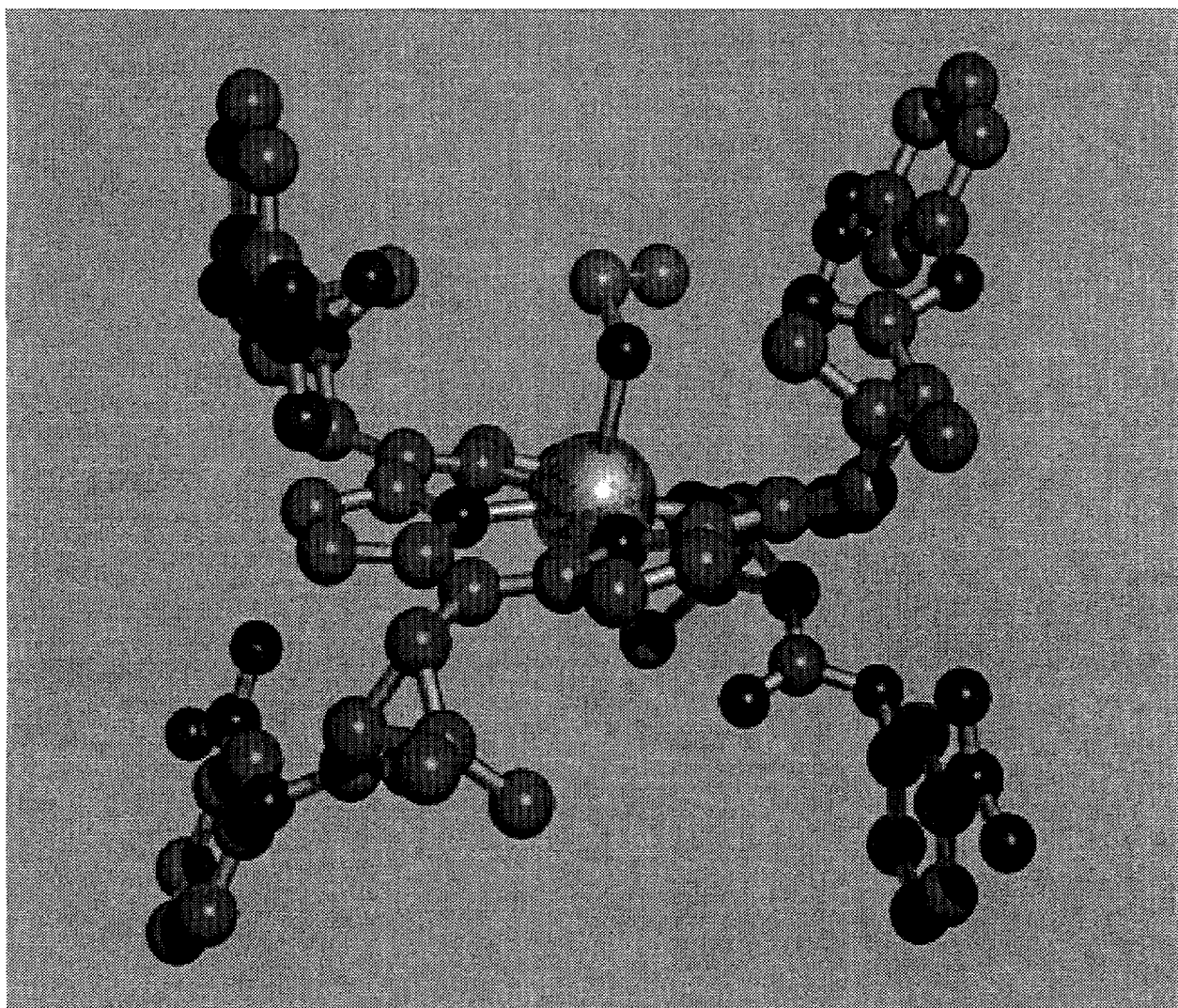
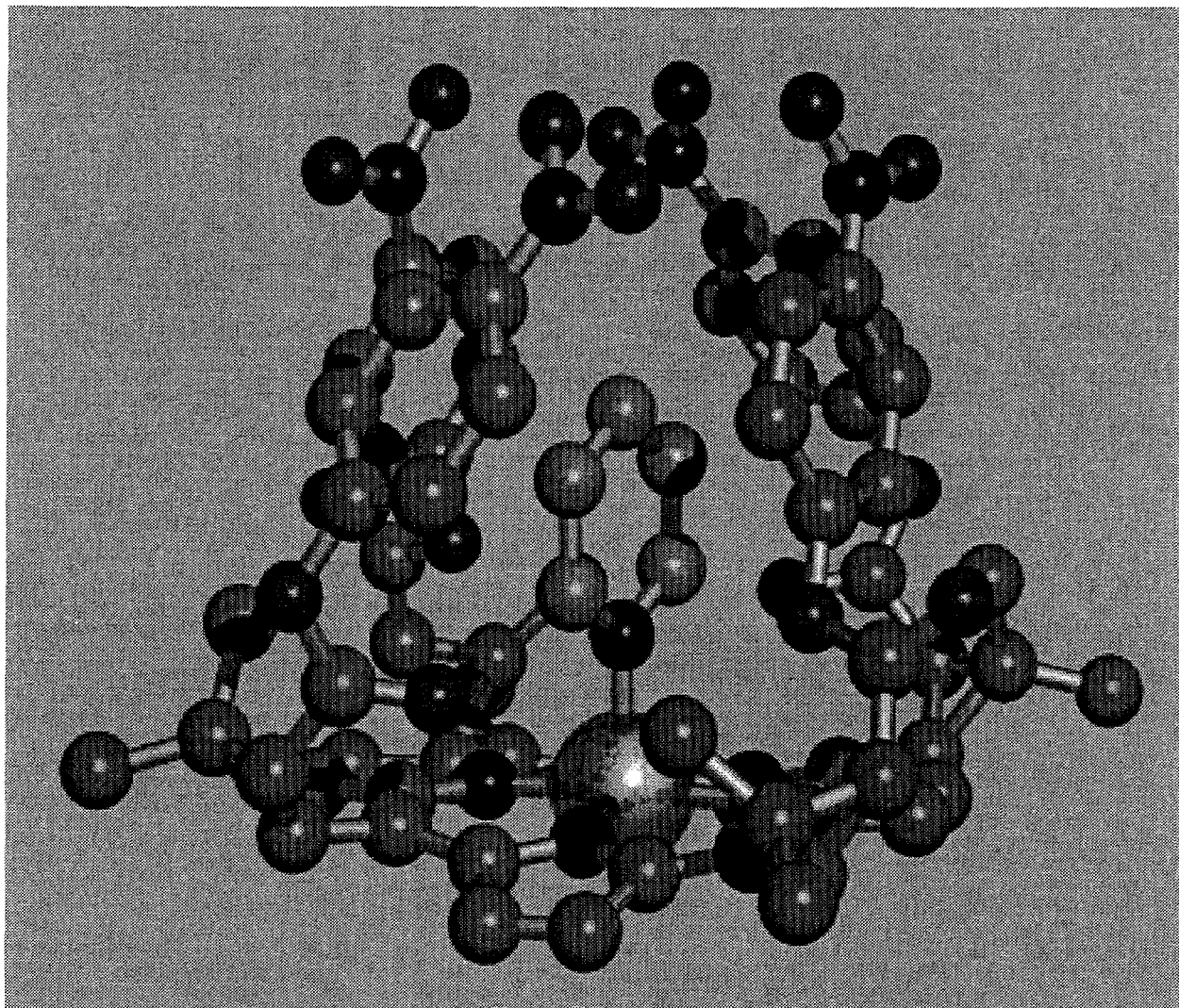


**Figure 4:** Closed configuration of “Venus flytrap” porphyrin due to addition of pyridine.



DISTRIBUTION:

3	MS-0710	T. Nenoff
1	MS-0710	A. Sylwester
1	MS-0710	S. Thoma
3	MS-1349	J. Shelnut
1	MS-1349	S.-L. Jia
1	MS-1349	Y. Qiu
1	MS-1349	J. Zhang
1	MS-1349	A. Hurd
1	MS-1349	J. Brinker
1	MS-1407	D. Sasaki
1	MS-1421	P. Provencio
1	MS-1421	G. Samara
1	MS-9018	Central Technical Files, 8940-2
2	MS-0899	Technical Library, 4916
1	MS-0619	Review and Approval Desk, 15102

For DOE/OSTI